

Three-Dimensional Organization of *Drosophila melanogaster* Interphase Nuclei. I. Tissue-specific Aspects of Polytene Nuclear Architecture

Mark Hochstrasser and John W. Sedat

Department of Biochemistry and Biophysics, University of California, San Francisco, California 94143

Abstract. Interphase chromosome organization in four different *Drosophila melanogaster* tissues, covering three to four levels of polyteny, has been analyzed. The results are based primarily on three-dimensional reconstructions from unfixed tissues using a computer-based data collection and modeling system. A characteristic organization of chromosomes in each cell type is observed, independent of polyteny, with some packing motifs common to several or all tissues and others tissue-specific. All chromosomes display a right-handed coiling chirality, despite large differences in size and degree of coiling. Conversely, in each cell type, the heterochromatic centromeric regions have a unique structure, tendency to associate, and intranuclear location. The organization of condensed nucleolar chromatin is also tissue-specific. The tightly

coiled prothoracic gland chromosomes are arrayed in a similar fashion to the much larger salivary gland chromosomes described previously, having polarized orientations, nonintertwined spatial domains, and close packing of the arms of each autosome, whereas hindgut and especially the unusually straight midgut chromosomes display striking departures from these regularities. Surprisingly, gut chromosomes often appear to be broken in the centric heterochromatin. Severe deformations of midgut nuclei observed during gut contractions in living larvae may account for their unusual properties. Finally, morphometric measurements of chromosome and nuclear dimensions provide insights into chromosome growth and substructure and also suggest an unexpected parallel with diploid chromatin organization.

IN a polytene interphase nucleus, chromosomes undergo repeated rounds of DNA replication without nuclear division. The homologous chromatids remain in close lateral alignment, rendering chromosomes with distinctive banding patterns visible in the light microscope. These nuclei provide a useful model system for directly analyzing interphase chromosome organization. Previously, we determined the spatial organization of chromosomes in a set of nuclei from *Drosophila melanogaster* salivary glands, which have the highest level of polyteny in the larva (22, 34). Characteristic packing motifs were found, including a polarized (Rabl) orientation of chromosomes across the nucleus, separation of chromosomes into noninterwound spatial domains, nearest-neighbor packing of the metacentric autosome arms, high-frequency contacts between a specific set of loci and the nuclear surface, invariant apposition of the aggregated centromeric regions (the chromocenter) to the nuclear surface, and a striking right-handed coiling chirality that does not require homologue pairing. Despite these nonrandom features, precise chromosome configurations appear not to be specified. Thus, while the folding of chromosomes is not identical in every salivary gland cell, several other facets of their organization are quite well defined.

To what degree the properties of the large, densely packed, salivary gland nuclei reflect structural features of all polytene nuclei or, instead, are a function of ploidy or cell type is unknown. Many tissues in *D. melanogaster* larvae are polytenized but generally not to the same high level as in salivary glands. It would be possible to address several issues raised by the salivary gland data in a comparative analysis of chromosome organization in different tissues. Central questions include whether a tissue-specific set of loci localizes to the nuclear surface in each differentiated cell type and whether a right-handed chirality typifies the coiling of all polytene chromosomes. In addition, chromosomes in other tissues may have more regular spatial configurations than in the salivary gland, particularly because variable cell types could not be rigorously ruled out in the latter tissue. Analysis of lower polyteny nuclei should also help clarify to what degree results from polytene tissues can be extrapolated to differentiated diploid cells. Finally, correlations of specific organizational features with cell type can provide clues about their possible functional significance.

Such a comparative analysis has now been done. It was first necessary to identify tissues with sufficient polyteny and optical clarity to permit a three-dimensional study. Existing cytological methods were refined so that less-polytenized nuclei could be analyzed. Three wild-type larval tissues that have been subject to little or no previous study provided the

Dr. Hochstrasser's present address is Dept. of Biology, 16-520, Massachusetts Institute of Technology, Cambridge, MA 02139.

material on which the present work is based. The data described here should therefore be of general utility for studies of polytene chromosome structure and function.

In this report, nuclear architecture in salivary gland, prothoracic gland, hindgut, and middle midgut nuclei is compared. First, such global properties as chromosome size, packing density, and coiling, and aspects of chromosome and nuclear growth inferred from them, are described. This is followed by a comparison between cell types of local regions of the genome, in particular, centric heterochromatin and nucleolar chromatin. From the similarities and differences between cell types, we make inferences about the mechanisms and physical properties of chromosomes and nuclei that result in the organizational motifs observed. The following article (21) focuses on aspects of chromosome spatial organization that have been hypothesized to be involved in the control of gene expression. Together, the results provide a precise description of interphase chromosome organization in polytene nuclei. The many similarities to diploid nuclei suggest that the data are relevant to these cell types as well. The results thus provide a structural framework for general models of nuclear architecture and the functional organization of the genome.

Materials and Methods

Tissue Preparation

Either of two wild-type Oregon-R stocks were employed. One, obtained from S. Beckendorf (University of California, Berkeley), had been made isogenic for the X chromosome (referred to as OR-isoX in reference 22). The models made from prothoracic glands and hindgut were from OR-isoX larvae, whereas both stocks were used for midgut (and salivary gland) nuclei reconstructions. Flies were raised on standard commmeal food supplemented with yeast in uncrowded bottles. The bottles were either left at 16°C for the entire period to third instar or were transferred to 16°C after allowing egg laying for several days at 25°C. Growth at low temperature increases the fraction of nuclei that reach higher levels of polyteny (18). It does not alter chromosome organization inasmuch as the salivary gland nuclei from Hochstrasser et al. (22) that were from OR-isoX larvae raised at 16°C did not differ in any measure from those of larvae raised at 25°C, including average chromosome dimensions.

Tissues were prepared for optical-sectioning microscopy as follows. The anterior end of the larva was removed by grasping behind the mouthhooks with a pair of jeweler's forceps and pulling away the anterior tissue with another. Part of the viscera was ejected through the opening created; the rest was gently pushed out by running lightly clamped forceps along the body from the posterior tip. The interconnected organs were then gently cut and teased apart with needles to isolate the desired tissue. Most of the gut is knotted together by tracheal tubes, and some must be severed to get at the "large cells" of the middle midgut. These are located right at the bend between the Ia and Ib segments of the midgut (50). The midgut was cut in positions far from the bend, and the loop of intestine was carefully removed. The hindgut usually hangs free of the gut and could be viewed without cutting it away. For schematic illustrations of the larval gut, see references 17 and 40. To minimize perturbations, ring glands were examined without separating them from the brain and imaginal disks. Aggarwal and King (1) provide drawings of the ring gland and the location of prothoracic cells within it.

Buffer and Staining Conditions

Gut tissues were transferred to a drop of buffer containing 3–5 µg/ml of the DNA-specific fluorescent dye 4',6-diamidino-2-phenylindole (DAPI)¹ and were mounted in this solution. Ring glands were stained for 10–20 min in 20 µg/ml DAPI and mounted in DAPI-free buffer. DAPI is a nonintercalating dye that does not appear to perturb chromosome structure. Different staining protocols were used with the different tissues because of differences

1. *Abbreviation used in this paper:* DAPI, 4',6-diamidino-2-phenylindole.

in the rate of dye uptake. Samples were mounted under bridged coverslips sealed with paraffin oil and were immediately mounted on a computer-controlled Zeiss Axiomat inverted microscope (Carl Zeiss, Inc., Thornwood, NY). Optical sections of nuclei were collected as described previously (22, 34). After the initial 256-frame video averaging of the fluorescence images to reduce the effect of camera noise, no image processing of any kind was used on any of the nuclei discussed in this report.

The buffer used with the gut tissues was the following formulation of Buffer A (8, 45): 15 mM Hepes, 0.15 mM spermine, 0.5 mM spermidine, 80 mM KCl, 15 mM NaCl, 0.1 mM EGTA, 0.5 mM EDTA, 15 mM 2-mercaptoethanol, pH 6.8. All other buffers that were tried, including physiological ones, lead to severe shortening of the gut that compressed the nuclei into flat crescent shapes. In the serum-free physiological medium D22 (14), this contraction occurs but is gradual. The initial appearance of nuclei in this case is the same with regard to nuclear shape and general chromosome layout as those in buffer A. Ring glands were isolated and mounted in D22 medium. Buffer A was not suitable in this case because the chromosomes tended to contract toward the nuclear surface with time, whereas in D22 medium, their positions were stable for many hours. For midgut and prothoracic glands, examination of nuclei in living larvae (see below) indicated that the chromosome organization described for these tissues reflects the *in vivo* situation.

Histological Assays

To verify that the middle midgut cells studied here were indeed the "large cells" (40) and not the copper accumulating calycocytes located just proximal to them, larvae fed on food mixed with copper sulfate were dissected and their intestines were subjected to a histochemical assay for copper using diethyl dithiocarbamate (17). The distinctive group of cells immediately proximal to the Ia/Ib bend developed a characteristic yellow-brown precipitate because of copper uptake; the large cells described in this report, which are right at the bend, did not.

Approximate cell counts were made as part of the characterization of midgut and prothoracic gland tissues from the stocks used in this study. 12–16 "large cell" midgut nuclei could be counted in DAPI-stained whole mounts, and 35–41 prothoracic gland nuclei were counted in orcein-stained preparations. These are comparable to published values: 14–18 (40) and 40 (23), respectively. All the tissues studied here undergo histolysis well after the stage at which they were analyzed (42).

Model Building and Mapping of Cytology

The three-dimensional paths of chromosomes were traced as described previously using the interactive modeling program IMP (32–34). Because midguts occasionally move slightly on the slide due to residual muscle activity, data from the same nucleus were taken at two different times to test for possible changes in chromosome dispositions. From the models made from each data stack, it could be shown that despite a slight reorientation of the nucleus relative to the objective microscope lens between time points, they were indistinguishable by all the quantitative parameters described in this and the accompanying paper.

The general banding pattern is very similar between tissues, but there are differences in puffing, relative band spacings, and the appearance of cytological landmarks. These differences made it extremely difficult, at least initially, to identify bands in intact nuclei, so photograph montages of squashed, orcein-stained chromosomes from each tissue were prepared and used as guide maps (20).

The surface of the single large nucleolus in prothoracic gland cells could be traced. This was done in either of two ways. In the first, the modeling program was modified so that the outline could be represented by more than the 512 points used for each chromosome arm. Thus, when the nucleolar outlines are traced in each section and are connected into a set of linked ellipses, the nucleolar surface will be adequately sampled. In the second, the nucleolus is modeled by a set of interpenetrating disks, each the thickness of an optical section (Mathog, D., and J. W. Sedat, manuscript submitted for publication; Fig. 3 a). Both methods yield the same result when measuring the distances between chromosome loci and the nucleolus; the latter method also allows nucleolar volume to be measured conveniently.

Morphometric Measurements and Quantitative Model Analysis

Chromosome widths were measured at 10 reference bands, two from each chromosome arm, that were unpuffed in all tissues (8E1, 13B1, 22A1, 29E1,

45A1, 55A1, 63A1, 67F1, 87B1, and 89A1; 67F1 was slightly puffed in a few of the salivary gland nuclei). At least seven and generally eight to nine of these bands could be measured in each nucleus. The 15 salivary gland nuclei were from the unfixed nuclei discussed in Hochstrasser et al. (22). The prothoracic gland polyteny levels inferred from bandwidth measurements (see Results) are somewhat higher than Welch's (53) values from Feulgen cytophotometry. His values for other tissues also appear to be systematically lower than in other studies (e.g., 28). Polyteny level can vary with genetic background (53). In addition, we always select the largest nuclei in the tissue, so our values will be strongly biased toward the highest levels.

Euchromatic chromosome arm lengths were measured between the following endpoints: X (1A–20A), 2L (21A–40A), 2R (60F–42A), 3L (61A–80A), and 3R (100F–82A) (6). Chromosome volumes were approximated by the volume of a cylinder (chromosomes being radially symmetric in cross section; reference 36) whose width equaled the average width of the set of reference bands and whose length equaled the sum of the model lengths of the five major arms. The small fourth chromosome could frequently be modeled but was not included in any of the size calculations. Nuclear (and nucleolar) volumes were calculated by placing a cube of the smallest possible size around the model and picking 10^4 random points within the cube. By multiplying the known volume of the cube by the fraction of the points that fell within the surface of the model, the nuclear volume was obtained (Mathog, D., and J. W. Sedat, manuscript submitted for publication). Similar values were obtained if the number of random points was increased 10-fold. The surface of the model is defined by a multifaceted polyhedron in which the model is inscribed (32). Because the models are drawn roughly down the center of the chromosomes, the calculated nuclear volume is less than the actual volume. To correct for this, each facet in the polyhedral surface was moved outwards by a distance equal to the average chromosome radius determined from the bandwidth measurements.

Midgut nuclear shape is generally that of a flat oblate ellipsoid. A measure of this flatness was made from the ratio of the maximum diameter measured on the displayed chromosome model to the maximum distance between any two model points along the direction in which the model is flattest, the two axes being roughly orthogonal. The latter distance is equal to the largest of the dot products between the unit vector pointing in the short axis direction and the vector between each pair of model points. The average chromosome width was added to both long and short axis values in each nucleus (see Table I).

Triple product and unpacking ratio calculations were done as before (22, 34). In this paper, we have summed the values from either of these metrics over all chromosome arms because there were no major differences between arms. Also, plots of these parameters vs. cytological position did not reveal any well-defined local regularities. Logarithmic plots of nuclear volume vs. chromosome volume were analyzed by linear regression (see Table IV). The linear correlation coefficients were 0.88 (prothoracic gland), 0.77 (midgut), and 0.92 (salivary gland). All are statistically significant correlations. Regression lines were compared by covariance analysis, and mean values of different measurements were compared with Student's *t* test (44).

In Vivo Observations of DAPI-stained Tissues

Third-instar larvae, either crawling at the edge of or in the food layer, were washed in saline, etherized, mounted on double stick tape, and then microinjected through the posterior end with an estimated 1–2 μ l of a solution of 200 μ g/ml DAPI in insect saline. Injected larvae were mounted on a slide under a firmly taped coverslip. Larvae were viewed with minimal irradiation on a Zeiss Universal microscope connected to a Chalnicon camera (DAGE-MTI) and a Sony videocassette recorder. The lamp aperture was reduced and the camera was operated at high gain. Prolonged exposure of midgut cells even at these low levels appeared to lead eventually to reduced gut contractions and pycnosis of nuclei; therefore, nuclei were generally examined for only a few minutes. For tracking nuclei in isolated midguts for longer periods, a high-sensitivity SIT camera (DAGE-MTI) was employed. Photographs were taken from stop-frame video images on an RCA television monitor.

Electron Microscopy

The same buffers as above were used for tissue dissections. Tissues were either fixed at room temperature for 1–2 h in 3.7% formaldehyde prepared from paraformaldehyde (Polysciences) followed by 2% glutaraldehyde (Polysciences, Inc., Warrington, PA) for 4 h or were fixed for 2–4 h in 2% glutaraldehyde at room temperature and then overnight in fresh fixative at 4°C. In the latter case, tissues were also postfixed for 2 h in 2% OsO₄. All

fixatives were in buffer A. Dehydration through a DMSO series was followed by embedding in Spurr's resin (Polysciences, Inc.). Blocks were sectioned with glass knives, and random or serial gold sections were collected on 100–150-mesh copper grids that had either been coated with or rapidly dipped in Formvar (55). Sections were stained with 2% uranyl acetate (either aqueous or in 50% ethanol) and ~0.5% lead citrate. Specimens were viewed at 80 kV with a 30- μ m objective aperture in a Philips EM400 microscope (Philips Electronic Instruments, Inc., Mahwah, NJ).

Results

It is generally held that the only wild-type *D. melanogaster* tissue of sufficient polyteny for routine cytogenetic analysis is the salivary gland (3). The single detailed study of polytene chromosomes in another wild-type tissue is by Richards (41), who analyzed part of the fat body. Unfortunately, the cells are almost completely opaque in whole mounts. Other species of *Drosophila* such as *D. hydei* do have larger polytene chromosomes in other tissues (3). On the other hand, because of the wealth of cytological and genetic information available for *D. melanogaster*, it would be of great advantage if a comparative analysis of chromosome folding could be based in this species. We therefore undertook a systematic search in several stocks for candidate tissues with suitable optical properties and levels of polyteny (20). Cells in several larval tissues proved to be of high polyteny: the large cells of the middle midgut (40), the hindgut, and the prothoracic gland.

The prothoracic gland forms part of the larval ring gland and is the site of α -ecdysone synthesis. This steroid is the immediate precursor of the growth and moulting hormone, 20-hydroxyecdysone (1). The large cells of the midgut are of ill-defined function. Ingested food is thought to undergo acid hydrolysis in this part of the gut (17). The large cells appear to develop from the tip of the endodermal posterior midgut invagination (40). The role of the hindgut, the final segment of the intestinal tract, is also not well understood, although in some insects a general secretory function has been ascribed to it (see reference 50); it forms from the proctodeum, an ectodermal rudiment.

General Description of Nuclei from Different Tissues

Three-dimensional chromosome models were constructed from stacks of optical sections of unfixed, unembedded, DAPI-stained nuclei from the different tissues. 25 middle midgut nuclei from 15 female and 2 male larvae were reconstructed; the majority of these nuclei were from the two to four cells right at the Ia/Ib bend (50). 11 prothoracic gland nuclei, most located near the corpus allatum, from seven female larvae and four nuclei from a patch of distal hindgut cells in one female larva provided the other reconstructions described in this report. Examples of unprocessed optical sections of nuclei from each tissue are displayed in Fig. 1 (for sections of salivary gland nuclei, see reference 34).

Prothoracic gland chromosomes are tightly coiled within a generally spheroidal nucleus ~22–25 μ m in diameter; a large nucleolus usually occupies the central zone of the nucleus. Hindgut chromosomes are also tightly coiled in many regions, although long, straight stretches are not uncommon; these nuclei are also usually spheroidal or slightly ellipsoidal with similar diameters to prothoracic gland nuclei. In contrast, the large-cell midgut nuclei form flat ellipsoids. The

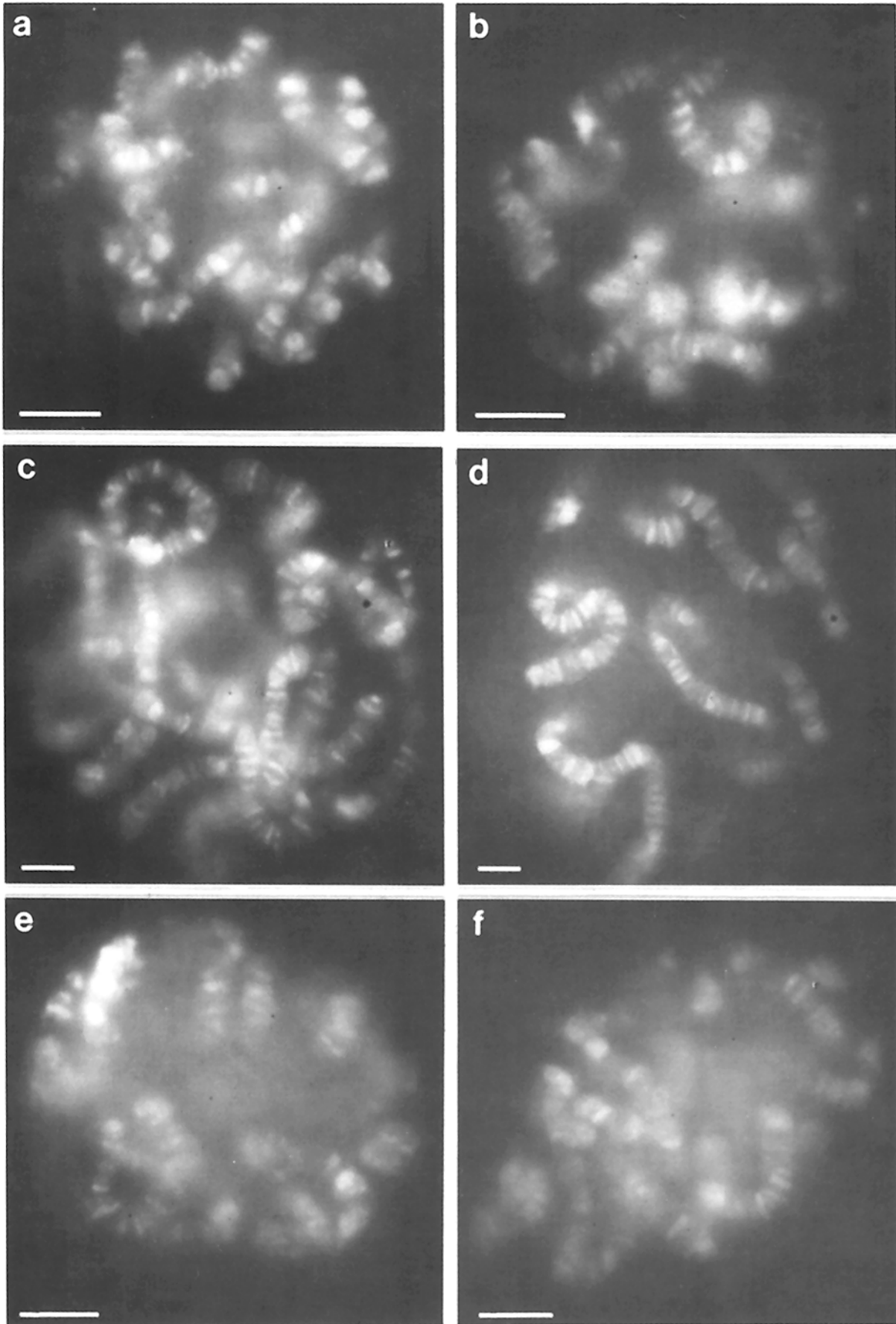


Table I. Average Middle Midgut Nuclear Diameters

Long axis length*	Short axis length*	Long axis/short axis
μm	μm	
44 ± 5	20 ± 4	2.3 ± 0.4

Data given \pm standard deviation.

* Values from measurements of models to which the average chromosome diameter for each nucleus has been added (see Materials and Methods).

long axis can exceed 50 μm in length and, on average, is 2.3 times longer than the short axis (Table I). Midgut chromosomes are also unusually straight, often with only a few true gyres in the entire nucleus. In comparison, the nuclei of the salivary gland are $\sim 35 \mu\text{m}$ wide and contain densely packed, coiled chromosomes (22, 34).

Chromosome Size and Packing Density in Different Tissues

With the ability to identify the chromosome banding pattern in intact tissues, it was possible for the first time to obtain measurements of chromosome dimensions under approximately in vivo conditions. Fig. 2 is a histogram of mean chromosome widths measured in 55 nuclei, none of which had been fixed or embedded. The same 10 reference bands were measured in each nucleus (Materials and Methods). Tables II and III provide data on several other nuclear size parameters.

Studies comparing (squashed) chromosome bandwidth to DNA content indicate that width is a fairly accurate indicator of degree of polyteny (18, 28); it increases by a factor of $\sim\sqrt{2}$ with each round of replication. Three of the peaks in the histograms fit the prediction well (peaks centered at 1.5, 2.1, 3.1 μm), but the final peak in the salivary gland nuclei (3.5 μm) is at a lower width than expected. Chromosome width in the largest DNA class observed by Hartmann-Goldstein and Goldstein (18) also fell below the predicted increase. From these data, it seems most likely that a range of four levels of polyteny is represented in the present sample of nuclei.

A comparison of approximate chromosome volumes (Materials and Methods) presents a similar picture. There is an 11-fold range in average chromosome volume between nuclei in the largest putative polyteny class and those in the smallest. This is close to the $2^3 = 8$ value expected for

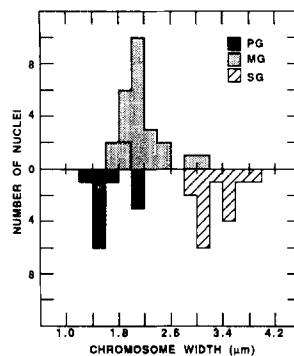


Figure 2. Average chromosome widths from four polytene tissues. Chromosome widths were measured at the same 10 prominent, unpufted bands (see Materials and Methods). Midgut (MG; 25 nuclei) and hindgut (4 nuclei) widths are shown above the central horizontal axis, prothoracic gland (PG; 11 nuclei) and salivary gland (SG; 15 nuclei) widths in inverted orientation below it. The hindgut chromosome diameters overlap the midgut widths in the

1.4–1.8- μm size interval (indicated by broken lines); an assignment to a particular polyteny class cannot be made from the limited hindgut data.

three doublings, assuming chromosome volume is proportional to chromosome dry mass and, therefore, DNA content (28). Although DNA content has not been directly measured, reference to the data from Laird et al. (28) indicate the largest salivary gland nuclei should be in the 2048C class, i.e., 10 rounds of endoreduplication. This would put the lower prothoracic gland size at 256C.

Chromosomes occupy a far greater fraction of the nuclear volume in salivary glands than in the other tissues (Table IV). The differences between all tissues are statistically significant. Interestingly, if nuclei from either prothoracic glands or midguts are divided into putative polyteny classes (Fig. 2), the volume fraction occupied by chromosomes in the more highly polytenized nuclei is significantly higher than in the smaller ones (Table IV). Chromosomes in these tissues thus increase in volume more rapidly than do the nuclei in which they reside. In contrast, chromosomes in the two apparent polyteny classes in salivary glands occupy the same nuclear volume fraction (nuclei were divided between those with a mean bandwidth greater than or equal to 3.3 μm and those below this). These relative trends are confirmed by an allometric analysis of nuclear versus chromosome volumes (Table IV, last column). Another measure also suggests that there is a change in the properties of chromosome and nuclear growth at the highest levels of polyteny. In both prothoracic gland and midgut nuclei, chromosome width correlates with chromosome length ($r = 0.71$, $P < 0.02$; $r =$

Table II. Euchromatic Chromosome Arm Lengths*

Chromosome arm	Prothoracic gland	Hindgut	Middle midgut	Salivary gland
	μm	μm	μm	μm
X	85.2 ± 9.3	98.1 ± 0.5	113.8 ± 13.2	139.8 ± 4.7
2L	80.5 ± 10.0	98.9 ± 6.3	111.6 ± 19.0	142.4 ± 9.7
2R	73.6 ± 7.4	96.2 ± 5.5	111.9 ± 15.2	144.3 ± 7.8
3L	80.6 ± 6.4	106.8 ± 2.8	116.3 ± 13.6	153.9 ± 12.2
3R	103.1 ± 11.3	127.0 ± 8.2	142.0 ± 18.2	184.5 ± 11.5

Data given as mean \pm standard deviation.

* Chromosome arm endpoints given in Materials and Methods.

‡ Only the 22 female nuclei are included.

Figure 1. Sample optical sections from DAPI-stained polytene nuclei. (a and b) Prothoracic gland nuclei. (a) A nucleus from the low polyteny class; (b) a nucleus from the higher class. (c and d) Middle midgut large cell nuclei. (e and f) Hindgut nuclei. The sections shown in this and all other figures are computationally unprocessed images. Bars, 5 μm .

Table III. Size Characteristics of Polytene Nuclei

Property	Prothoracic gland	Hindgut	Middle midgut*	Salivary gland
Total euchromatic chromosome length (μm)				
Average (\pm SD)	423 \pm 41	527 \pm 19	604 \pm 73	765 \pm 35
Range	390-530	508-546	477-798	714-825
Nuclear volume (μm^3)				
Average (\pm SD)	5,783 \pm 1,297	6,429 \pm 1,134	19,480 \pm 7,618	18,850 \pm 4,443
Range	4,543-7,789	5,687-8,116	9,150-35,797	13,253-31,858
Nucleolar volume (μm^3)				
Average (\pm SD)	343 \pm 127	—	—	—
Range	201-586	—	—	—

* Only the 22 female nuclei are included.

0.74, $P < 0.001$, respectively), whereas this is not true in the salivary gland ($r = 0.22$, $P > 0.2$). Nuclear volume in all tissues is positively correlated with both chromosome volume and chromosome width but increases at different relative rates in different tissues (Table IV).

The dimensions recorded in Tables II and III and Fig. 2 do not agree with those from any previous investigation except the length measurements of lax salivary gland chromosomes made by Bridges (7). Most or all of the discrepancies are probably a consequence of the squashing and/or fixation steps required in these studies (4, 6, 18, 29). Squashing stretches chromosomes to an unknown extent, and fixation also generally alters chromosome and nuclear dimensions. For example, fixing salivary glands in 3.7% formaldehyde can shrink chromosome lengths by over 30% (Hochstrasser, M., unpublished data; Mathog, D., and J. W. Sedat, manuscript submitted for publication).

Chromosome Organizational Motifs Differ with Cell Type

The packing of salivary gland chromosomes is characterized by a number of regular motifs which includes a polarized (Rabl) orientation of chromosomes, with centromeres and telomeres segregated to opposite sides of the nucleus; invariant separation of chromosomes into nonintertwined spatial domains; and close packing of the arms of each autosome next to one another (22, 34). We argued that this is reminiscent of properties of chromosomes in mitotic telophase and thus may reflect what would be a remarkable degree of posi-

tional stability as the last mitosis in this tissue is completed by the 8th hour of embryogenesis (47). One prediction of this argument is that nuclei with lower levels of polyteny (and diploid nuclei) will share these motifs.

Prothoracic gland nuclei as many as four levels of polyteny below salivary gland nuclei fulfill the prediction. The nucleus model in Fig. 3 a is a representative example. In every nucleus, chromosomes lie in nonintertwined domains, and in every nucleus, chromosome arm 2L is next to 2R and 3L is next to 3R. As in salivary glands, no other pair of arms are regular neighbors. Finally, though the chromocenter in prothoracic gland nuclei is generally in the nuclear interior (see below), it is still possible to define a polarization axis running from the chromocenter to the telomeres arrayed on the opposite side of the nucleus. Such a Rabl or pseudo-Rabl orientation is seen in $\sim 73\%$ of the chromosomes, comparable to the $\sim 80\%$ figure found for salivary glands (22).

A very different packing is seen in the nuclei of almost all midgut cells (Fig. 3 b). All of the chromosome-packing rules just described are regularly violated in this cell type. It is rarely possible to define a polarization axis; centromeres and telomeres are found throughout the nucleus. Autosome arms are also in a wide range of relative positions. Most dramatic is the frequent intertwining of chromosomes. Fig. 3 b shows a clear example of intertwining between the X and 3R chromosomes; an optical section that includes this region is shown in Fig. 1 d. In a graphic example of intertwining, displayed in Fig. 4, 2R threads through a coil in 3L; the original optical sections reveal that the coil is tightly wrapped around 2R. Not every nucleus has such closely entangled chromosomes, but lesser encroachments are found in almost all the nuclei (see Fig. 3 b).

Hindgut nuclei appear intermediate in their preservation of telophaselike motifs. The model in Fig. 3 c comes closest to this description, although 3L and 3R do not follow the general centromere-telomere polarization. Examples of chromosome intertwining, less pronounced than those in the midgut, were found in two of the four hindgut nuclei. In summary, nuclei in the hindgut and especially the midgut often deviate from the telophaselike properties seen in the other tissues.

Chromosome Coiling Shows the Same Chirality in All Tissues

An unexpected result from our analysis of salivary gland chromosomes was the discovery of a marked asymmetry in

Table IV. Comparison of Chromosome/Nucleus Volume Ratios

Tissue	Presumptive polyteny class	Chromosome/nucleus (SD)	t	Slope \ddagger
Prothoracic gland	256C	0.13 (0.02)	5.43*	0.44
	512C	0.20 (0.02)		
Middle midgut	512C	0.11 (0.03)	4.00*	0.73
	1024C	0.18 (0.02)		
Salivary gland	1024C	0.34 (0.03)	—	1.07
	2048C	0.34 (0.03)		

* $P < 0.001$ (for difference between polyteny classes).

\ddagger Rate of increase in nuclear volume relative to chromosome volume as determined by linear regression from log-log plots of nuclear (y) vs. chromosome (x) volume (Materials and Methods).

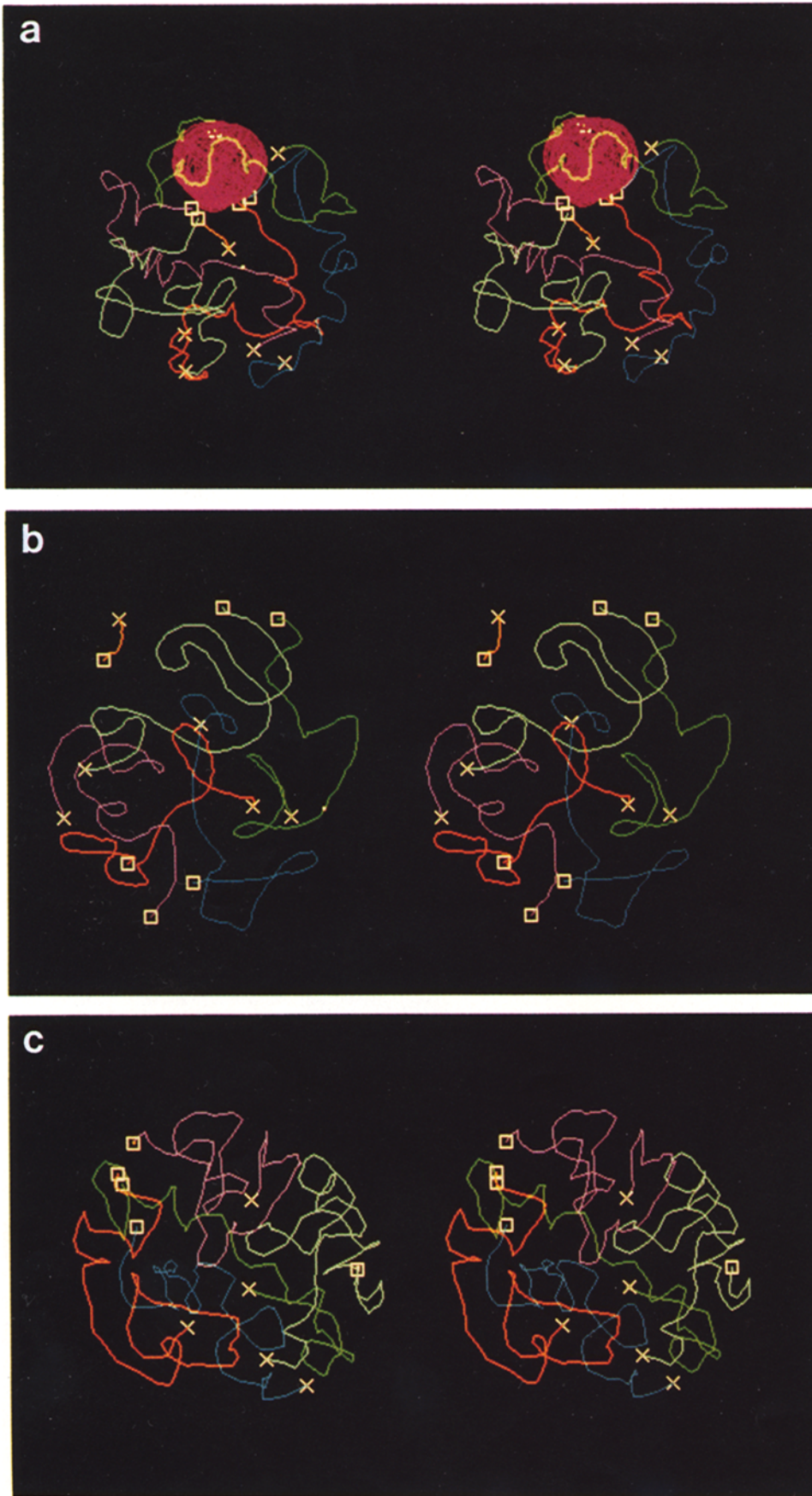


Figure 3. Stereopair chromosome models from each tissue. (a) Prothoracic gland nucleus. Each chromosome arm is color-coded as follows: X, green; 2L, red; 2R, blue; 3L, purple; 3R, light green; 4, yellow. The large pink ball represents the nucleolus. The crosses mark the telomeres of each chromosome arm and the squares their chromocentral endpoints. The X chromocentral endpoint is behind the nucleolus in this view. Because proximal heterochromatin is not modeled, the left and right arms of the major autosomes are not connected. (b) Middle midgut nucleus. The color code and markings are the same as in a. (c) Hindgut nucleus. The color code and markings are as above (chromosome 4 is not modeled). Different optical sections from this nucleus can be seen in both Fig. 1 e and Fig. 8 b. Model diameters in vertical direction are ~21, 49, and 22 μm for a-c, respectively. Handedness is correct for cross-eyed viewing.



Figure 4. Middle midgut chromosome arm 2R intertwined with 3L. 2R runs through a right-handed coil in 3L. Squares and crosses mark the chromocentral and telomeric endpoints, respectively, of each chromosome arm.

coiling direction: virtually all gyres are right-handed (22). Previous reports had maintained that left- and right-handed coils were equally likely (2, 4, 26). The source of this chirality is unknown, although its occurrence in asynapsed homologues indicates it is not due to homologous pairing. These results do not reveal whether the asymmetry is a fundamental property of all polytene chromosomes or when and how these chromosomes coil. These questions can be addressed with the present data.

Inspection of stereopairs (Fig. 3) demonstrates that all chromosomes in every tissue display the chirality first seen in salivary glands. Even in the generally straight or meandering midgut chromosomes, the infrequent gyres are nevertheless almost invariably right-handed. Direction of coiling can be directly determined in tightly coiled chromosomes. This is shown in Fig. 5 by successive optical planes through a solenoidal region in a hindgut chromosome. Finally, the unpaired X chromosomes in the three male midgut nuclei reconstructed as well as a long, asynapsed chromosome segment in another midgut nucleus could be roughly traced, and an apparent bias toward right-handed coiling was seen, in agreement with our observations in salivary glands.

A bias in coiling direction can be objectively demonstrated with the triple product calculation (5, 22, 34). This vector

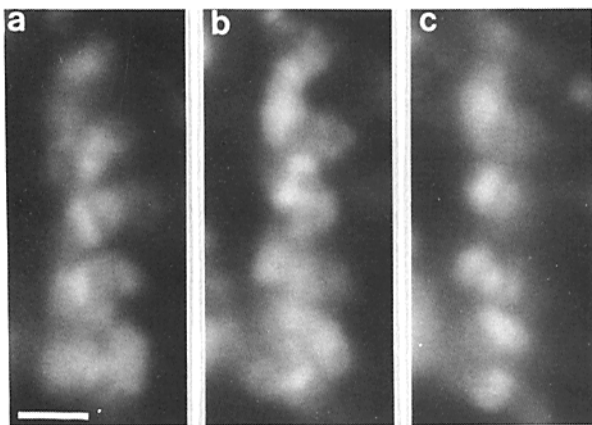


Figure 5. Right-handed solenoidal region of a hindgut chromosome. Successive optical planes, spaced at one-notch intervals on the microscope focus knob, through a tightly coiled chromosome segment. *a* is the top section. Pictures were taken on a Zeiss Universal microscope of a sample prepared in the same way as the hindgut from which the nuclear reconstructions were made. Bar, 2 μ m.

operation, $A \cdot (B \times C)$, where *A*, *B*, and *C* are successive vectors along a curve, will yield a positive scalar value if the vectors' relative orientations follow a right-handed screw, and vice-versa. Fig. 6 shows histograms of triple product values from each cell type summed over all chromosome arms in all nuclei. As can be seen, all the histograms are skewed toward positive values (compare to Fig. 3 in reference 22). Some differences between the plots, however, deserve comment. First, the midgut histogram shows a very large peak around 0; this is expected, given the unusually straight path taken by much of each chromosome. The coils in this tissue also tend to be flat, leading to triple product values near 0. Second, the ratio of positive to negative values is somewhat lower in the midgut nuclei. The reason for this is unclear in that this is not seen by visual inspection of models; it may well reflect the predominance of straight chromosomal segments and flat gyres rather than a real difference in chirality.

Different vector spacings were used for the calculations in different tissues because the chromosomes vary in length (Tables II and III) and in the characteristic dimensions of their coils. The tight coils in hindgut and prothoracic gland chromosomes would not be sampled adequately with the same vector spacing used for the much wider salivary gland chromosome gyres. Bending or coiling can be quantitated with an "unpacking ratio" parameter, which measures the ratio of the minimum distance between two points on the model path to the contour distance between these points; lower values indicate tighter coiling (32). For example, using a 7- μ m contour distance, prothoracic gland and hindgut chromosomes have mean unpacking ratios of 0.592 (± 0.012) and 0.643 (± 0.023), respectively, whereas for salivary gland

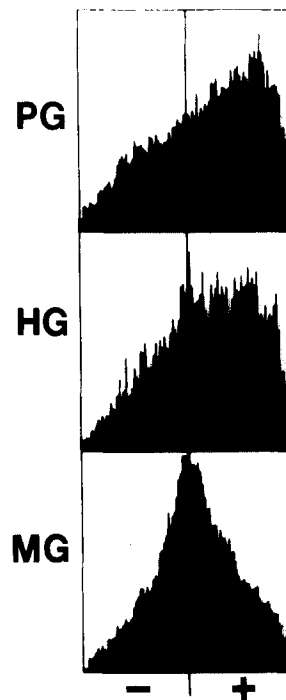


Figure 6. Triple-product histograms for chromosomes in three tissues. Triple-product values along each chromosome arm in every nucleus are histogrammed for each tissue. The triple product was calculated as described in the text. Positive values indicate right-handed coiling, negative values left-handed coiling. The vertical scale is arbitrary. Because of the different lengths of chromosomes in different tissues, different spacings between unit vectors were used to calculate the triple product; however, other spacings that are not extremely large or small yield the same qualitative results. Each individual chromosome arm also shows the skew toward positive values in each tissue. (PG) Prothoracic gland: 55 chromosomes; 4- μ m vector spacing. (MG) Middle midgut: 110 chromosomes (the three male nuclei were omitted); 5- μ m vector spacing.

(HG) Hindgut: 20 chromosomes; 4- μ m vector spacing. The ratio of positive to negative values using the indicated vector spacings are: 1.9 (PG), 1.9 (HG), and 1.3 (MG).

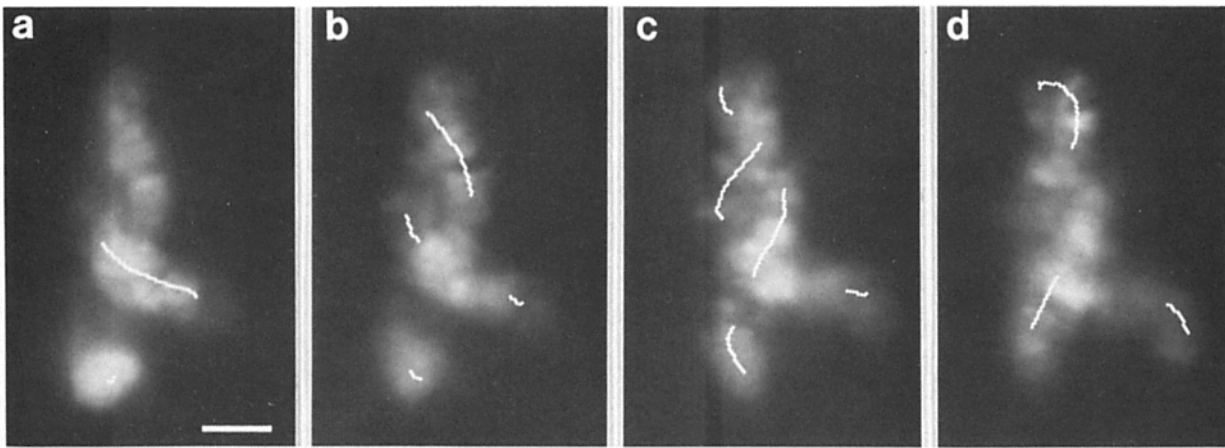


Figure 7. Left-handed plectonemic coil in chromosome arm 2R from a middle midgut nucleus. Successive optical sections are spaced at 1.4- μm intervals. *a* is the topmost section. Bar, 3 μm .

chromosomes, it is $0.778 (\pm 0.013)$. If prothoracic gland nuclei are divided into polyteny classes, the larger nuclei (0.605 ± 0.004) are less tightly coiled than the smaller ones (0.588 ± 0.009 ; $t = 4.035$, $P < 0.005$).

An unexpected variation to the "solenoidal" coiling described above has been found in a number of gut nuclei and one prothoracic gland nucleus. In these cases a segment of a chromosome arm folds back and twists about itself in a "plectonemic" or braidlike coil. If the forces leading to these interwound forms are related to those generating the right-handed solenoidal coils, one would predict that they will be left-handed. This is most easily understood using the node sign terminology introduced by Cozzarelli et al. (10); in both plectonemic and solenoidal coils, the nodes or self-crossings will be positive. This is exactly what is observed: in 11 examples of interwound helices, every one is left-handed. Fig. 7 shows a series of optical sections through one of them. The midgut model in Fig. 3 *b* shows an interwound region in chromosome arm 3L, while the hindgut model (Fig. 3 *c*) has an example in 3R. All of the examples have two nodes. As

outlined in Discussion, these plectonemic coils may shed light on the mechanism and timing of chromosome coiling.

Tissue-Specific Aspects of Nucleoli

Tissue-specific differences in the large-scale chromatin organization of several portions of the genome have been found. One of these is the condensed DNA found within the nucleolus. The density and distribution of the DAPI-bright material within the nucleolus differ in a characteristic way between the cell types studied (Fig. 8). The prothoracic nucleolus has a relatively diffuse DAPI fiber pattern (Fig. 8 *a*), whereas the hindgut nucleolus contains many small bright spots (Fig. 8 *b*). In contrast to either the diffuse fiber or punctate pattern of DNA staining, midgut nucleolar chromatin is most frequently seen as a fibrous clot of material (Fig. 8 *c*).

Nucleoli also vary in number between cell types. While prothoracic gland nuclei almost always have a single large nucleolus, representing 4–8% of the nuclear volume (Table III), midgut nuclei usually have multiple smaller nucleoli, frequently at the nuclear surface. The hindgut nucleus gener-

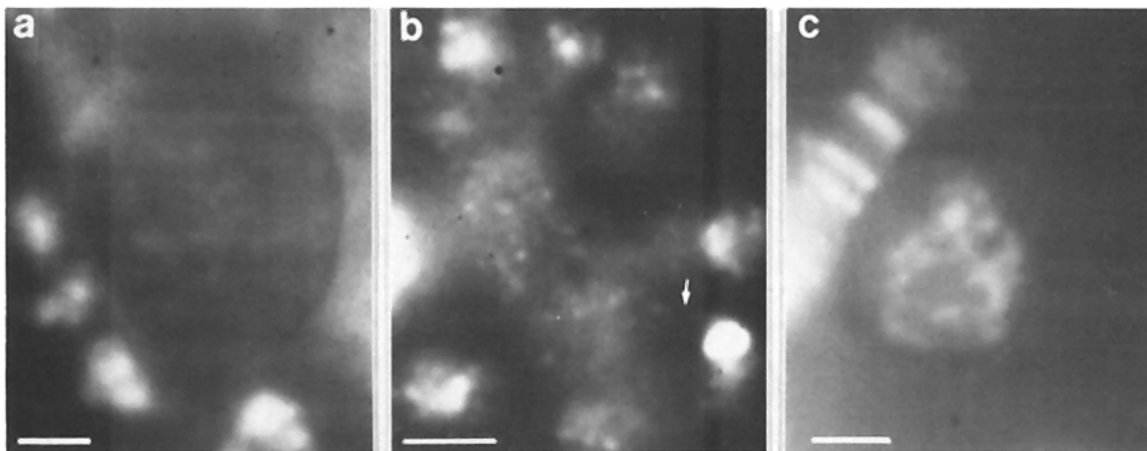


Figure 8. Organization of condensed nucleolar chromatin in three tissues. (*a*) Prothoracic gland nucleolus showing the diffuse fibrillar pattern of DAPI staining typical of this tissue. (*b*) Hindgut nucleolus showing punctate pattern of DAPI-bright staining. The arrow points to a thin fiber running from the proximal end of 3R to the nucleolus. (*c*) Midgut nucleolus containing a dense mat of thick DAPI-bright fibers. Bars, 2 μm .

ally contains a single large nucleolus, although more than one has been observed. One or two nucleoli are typical of salivary gland nuclei (46). The different nucleoli in midgut cells are often far apart from both each other and from the nucleolar organizer at the base of the X chromosome. This may reflect an extrachromosomal state of ribosomal DNA in this tissue.

Chromocenter Structure and Position is Tissue-Specific

The heterochromatic centromeric segments of each chromosome also have a tissue-specific organization. Their intranuclear location varies between cell types as well. In salivary gland nuclei, the centromeric regions of each chromosome usually aggregate into a single dense chromocenter; a small fraction of nuclei may contain two separate chromocenters (22). An invariant feature of salivary gland nuclear organization is the close association of the chromocenter, even when there is more than one, with the nuclear surface (22, 34).

The causes of centromere aggregation and of nuclear surface apposition are not known.

In contrast to salivary gland nuclei, the prothoracic gland chromocenter is usually in the interior of the nucleus (see Fig. 3 *a*). Because in telophase the centromeres are near one pole of the nucleus, at some point they must move toward the nuclear interior. It is interesting that something close to a Rabl orientation is nevertheless exhibited by these nuclei. Movement of centromeres away from the envelope has been documented in certain diploid cells (35). Optical sections from prothoracic nuclei in Fig. 9, *d* and *e*, highlight the distinctive morphology of the chromocenter in comparison with the chromocenter in salivary gland cells (Fig. 9, *a* and *b*). Rather than developing a dense reticulum of chromatin as in the latter examples, the prothoracic chromocenter forms a mat of thick, twisted fibers that is partly draped over the nucleolus.

Electron-microscopic examination of chromocenters from these tissues (Fig. 9, *c* and *f*) substantiates all of the above

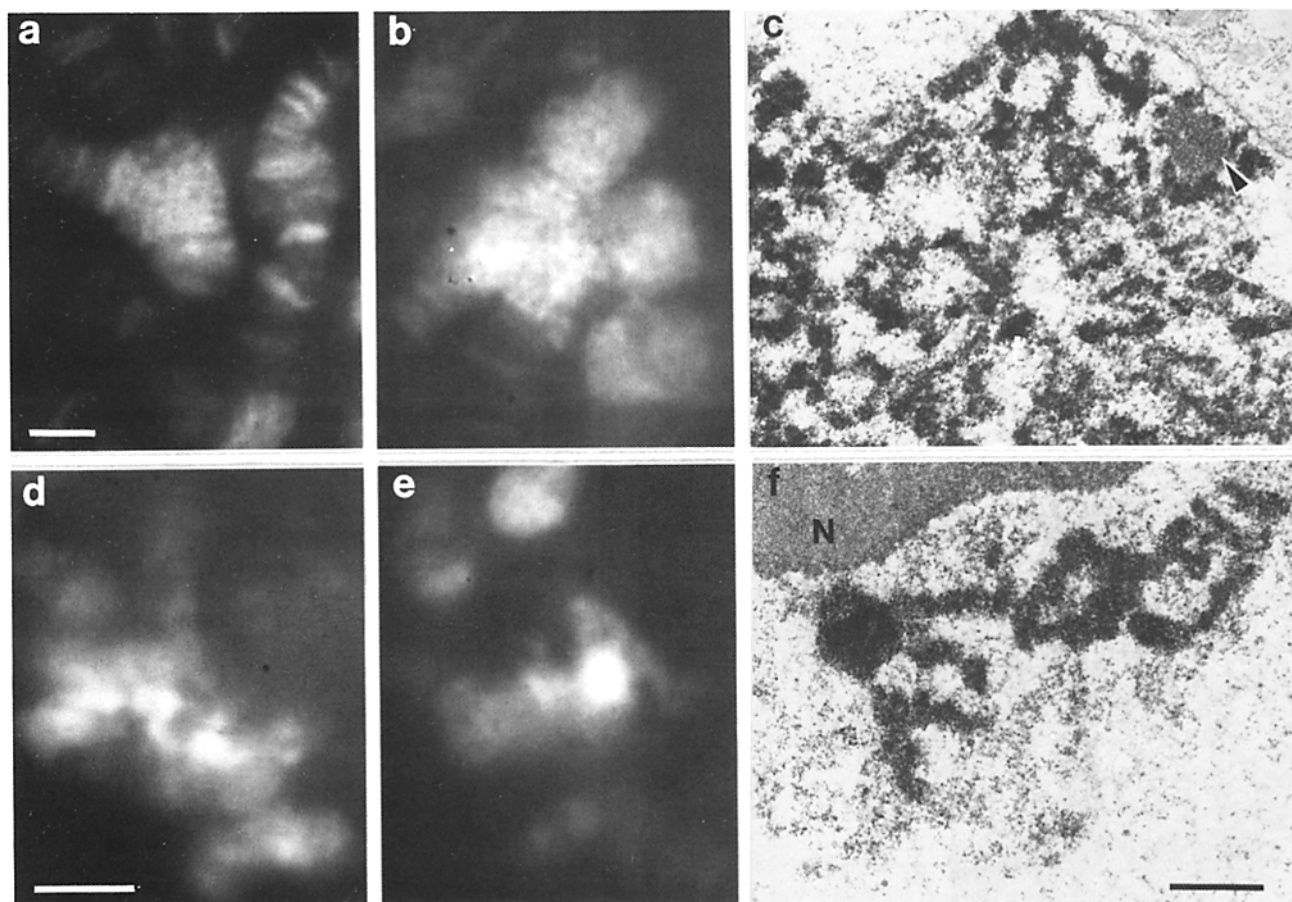


Figure 9. Chromocenter structure in prothoracic and salivary gland nuclei. (*a* and *b*) Optical sections of salivary gland chromocenters. In *a* only the centromeric region of chromosome 2 is seen. The other centric regions are located in another part of the nucleus, unconnected to this one. An irregular banding can be discerned. In *b* all the centromeric zones are aggregated, and the spongy chromatin structure is evident. (*c*) Electron micrograph of a section through a salivary gland chromocenter. Arrowhead points to the zone of α -heterochromatin (see reference 27). The reticular pattern of dense chromatin is β -heterochromatin; some irregular bands can be made out in the right of the micrograph. Short fibers run to the nuclear envelope between and/or to the edges of nuclear pores. (*d* and *e*) Optical sections of prothoracic gland chromocenters (associated with the nucleolus). *d* is from the lower polyteny class; *e* is from the higher one. (*f*) Electron micrograph of a prothoracic gland nucleus. The loose mat of twisted or zig-zagging fibers, which connect to the banded euchromatin at upper right, look very similar to the structures seen in the optical images. A cloud of small particles similar to those seen in the nucleolus (*N*) surround the chromocenter. Bars: (*a*, *b*, *d*, and *e*) 3 μ m; (*c* and *f*) 1 μ m.

points. The prothoracic gland chromocenter is in the nuclear interior, pressed against the nucleolus. It consists of large, well-separated fibers that join to the banded euchromatin and appears to have a coiled or zig-zag substructure. It is embedded in a mass of small granules that are presumably RNP particles (compare with nucleolar substructure); this suggests that β -heterochromatin (see Discussion) is transcriptionally active in this tissue. The salivary gland chromocenter shows the same spongelike mass of β -heterochromatin fibers that is seen in the light microscope. Moreover, it is pressed against the nuclear envelope with multiple fibers extending to the bilayer. The close packing of nuclear pores (Fig. 9 *f*) makes it difficult to tell whether the fibers attach to pore edges or to the lamina; the latter seems more likely from our micrographs to date.

Chromocenter structure and location are also distinctive in the gut tissues. Hindgut β -heterochromatin exists as long fibers terminating in dense masses; it is often not on the nuclear surface (Fig. 10 *d*). Midgut chromocenter structure cannot be easily classified because it varies widely both within and between nuclei. Typically, it appears as a loose network of short, criss-crossing fibers connecting denser clumps (Fig. 10, *a* and *b*). Sometimes it forms an irregular ladder of widely spaced bands (Fig. 10 *c*). Often, heterochromatic material that is not obviously connected to a chromosome is seen (*thin arrows* in Fig. 10 *b*).

Also varying greatly is the extent to which the different centromeric regions associate. In 24 of the 25 midgut nuclei reconstructed, at least two chromocenters were found. A portion of each chromocenter is usually, but not always, at the nuclear surface; this association appears much more tenuous than in the salivary gland. Differences in centric heterochromatin association and intranuclear position have been documented in diploid cells as well (24).

Most remarkably, gut chromosomes actually appear to be broken in half in many nuclei: the proximal endpoints of an autosome's arms are often far apart from one another, even on opposite sides of the nucleus. Integrity of centric heterochromatin segments appears not to be required in these tissues. In Fig. 3 *b*, for example, the proximal endpoints of the left and right arms of chromosome 3 terminate on the envelope on opposite sides of the midgut nucleus, almost 50 μm apart. Similarly, in the hindgut nucleus in Fig. 3 *c*, chromosome 3 is also severed (the 3R proximal end can be seen in Fig. 8 *b* to extend a short fiber to the nucleolus). It is sometimes difficult to tell if a thin fiber runs between chromocentral regions (midgut fibers as long as 20 μm have been measured), but at least one autosome appears split in 20 of the 25 midgut nuclei; chromosome 3 is the most frequently broken. It is conceivable that a very fine DNA thread connects the widely separated centric endpoints, but these nuclei are extremely clear optically and very thin fibers are readily ob-

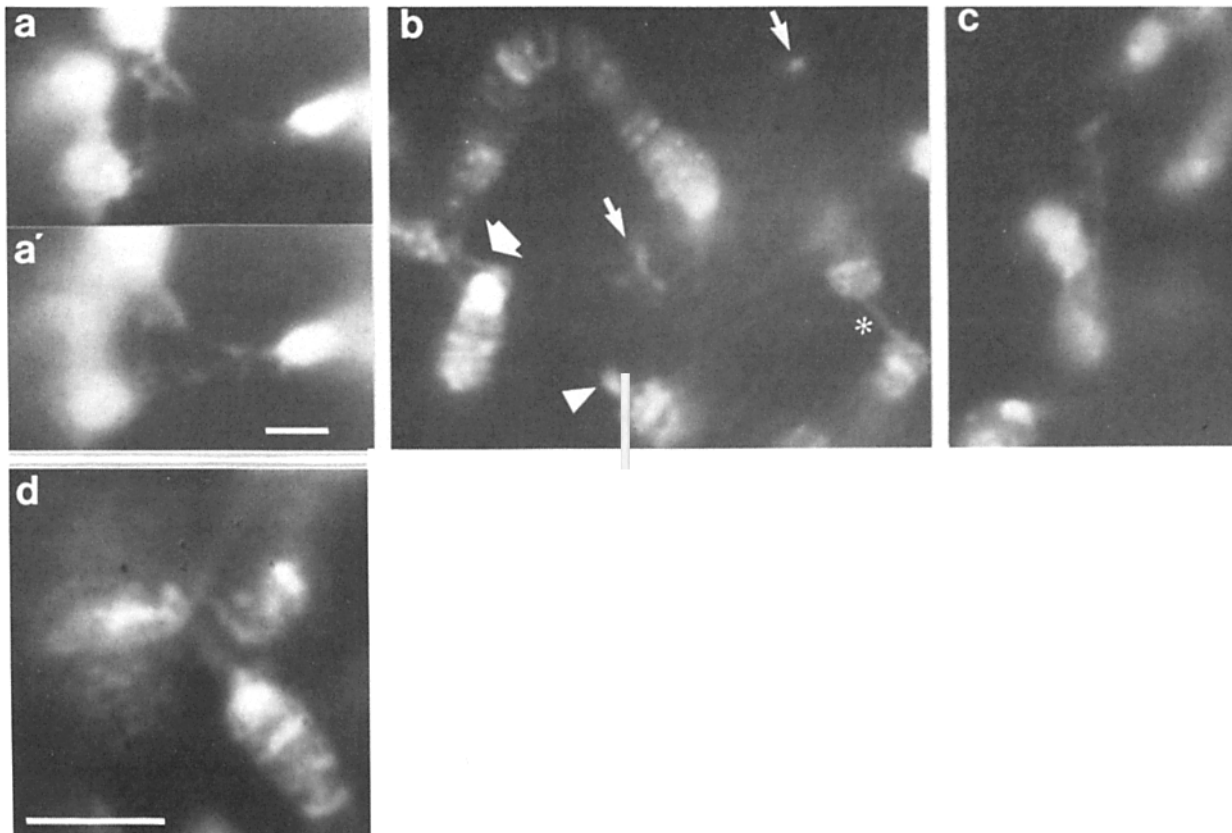


Figure 10. Chromocenter structure in middle midgut and hindgut nuclei. (*a-c*) Midgut chromocenters. *a* and *a'* are successive optical sections showing a network of heterochromatin fibers. In *b* the chromocentral endpoint of 3L (*arrowhead*) appears severed from that of 3R (*thick arrow*). Loose heterochromatin is indicated by thin arrows. The intercalary heterochromatin in 56F of 2R is pulled into a narrow fiber (*asterisk*). In *c* a portion of the X β -heterochromatin appears as a series of loosely linked bands and runs past a dense heterochromatic region of another chromosome. (*d*) Hindgut chromocenter. Long fibers, only partly in focus, run to a denser mass of heterochromatin near the nucleolus. Bars, 3 μm .

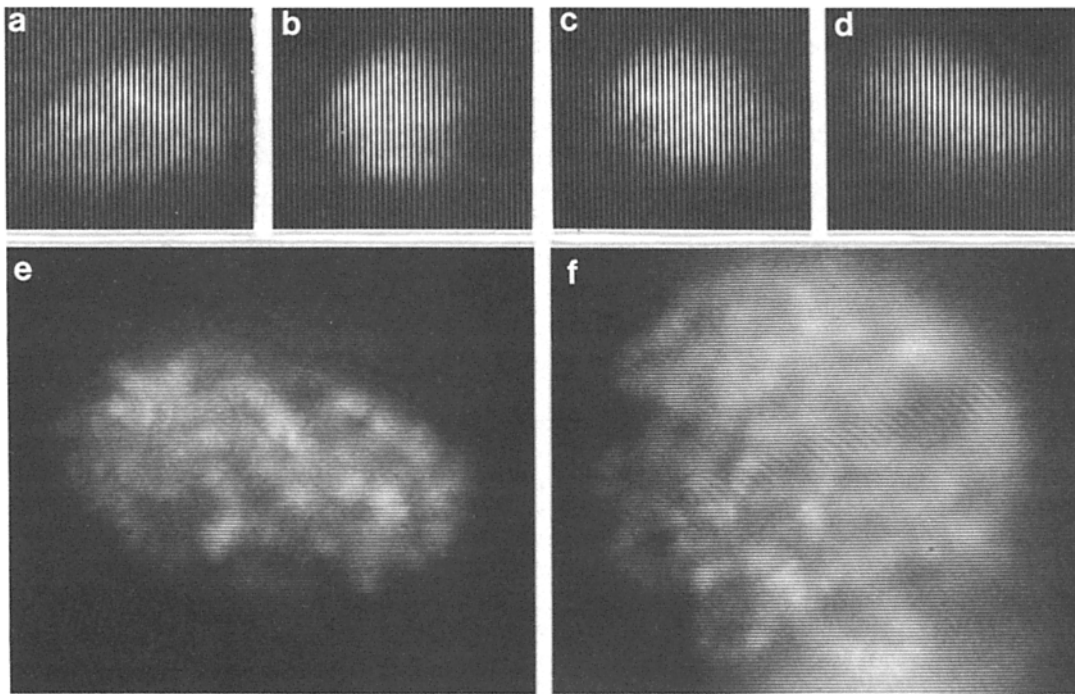


Figure 11. Appearance of middle midgut nuclei in living larvae. (a-d) A series of video images of the same nucleus over an interval of ~ 10 s taken on a 3/4-inch Sony videocassette recorder. A low-power ($\times 40$) objective lens was used for both increased depth of focus and ease of tracking nuclei. The series displays the dramatic changes in nuclear shape that occur during peristaltic contractions. (e and f) Different nuclei during phases with minimal local gut contraction taken with a $\times 100/1.3$ NA Neofluar lens. Despite the low resolution of the recording medium, the ellipsoidal shape of the nuclei and the straight or meandering paths of the chromosomes are apparent. Larvae were injected with a 200 $\mu\text{g}/\text{ml}$ solution of DAPI. Pictures of videoframe images were taken from a television monitor.

served between ectopically paired loci or at centric endpoints that send a fiber to the nuclear surface. We therefore doubt that such links always exist.

Euchromatic portions of chromosomes have never been observed to break. Weak points, however, which contain late replicating, tandemly repeated DNA sequences (56), are sometimes pulled out into thin fibers. Fig. 10 c (*asterisk*) shows an example at locus 56F, which contains the tandemly repeated 5S RNA genes. Other loci that have been observed as long fibers include 11A, 12F, 35CD, 36CD, and 89E, all which behave as weak points in salivary gland squashes.

Midgut Nuclear Shape Is Severely but Reversibly Deformed In Vivo

Because of the many unusual characteristics of midgut nuclei, we were concerned about *in vitro* distortions. For example, it is possible that by cutting the Ia/Ib gut segment free and isolating it in buffer A (Materials and Methods), the originally spherical nuclei collapse, pulling the chromosomes out into long straight stretches and perhaps tearing apart the chromocenter. The *in vivo* controls performed previously for salivary gland (22) could not be done with midgut nuclei as they are virtually invisible by bright field optics. As an alternative, we microinjected DAPI into the hemolymph of third instar larvae and examined the stained midgut within the living animal. Video recordings were used for documentation.

The following observations were made. The Ia/Ib bend undergoes particularly pronounced muscular contractions with occasional quiescent phases (also see reference 50). During

these latter periods, nuclei could be closely examined. The generally straight or meandering chromosomes and disk-shaped nuclei seen in isolated guts are indeed seen *in vivo* (Fig. 11, e and f). The large-cell nuclei are subject to severe deformations as is illustrated by the video time series, taken at low magnification, in Fig. 11, a-d. However, chromosomes are not simply floating freely and continuously rearranging; after a series of contractions, chromosomes appear to relax back to very similar configurations. This could be looked at more closely in guts isolated in buffer A without chelating agents (Materials and Methods). DAPI-stained guts will sometimes continue to contract under these conditions for 10-30 min. Here again, nuclei are strongly deformed by peristaltic contractions, and chromosomes, apparently shifting from these distortions, relax back to similar positions repeatedly, implying some kind of chromosome tethering (data not shown). It is not known whether, over hours or days, chromosome positions can gradually change.

Other tissues also take up DAPI in microinjected larvae. Prothoracic gland nuclei were examined and appeared similar to the description given in previous sections for this tissue. The hindgut is difficult to view within the larva, so a satisfactory *in vivo* description was not obtained.

Discussion

The spatial organization of *D. melanogaster* polytene chromosomes in four wild-type tissues, three that have not been studied previously, has been described. Nuclei in these samples appear to span three to four levels of polyteny, and

changes in chromosome packing could be studied not only as functions of cell type but also of chromosome and nuclear size. While certain features of nuclear organization were found in common among all nuclei, pronounced tissue-specific but polyteny-independent differences were found in nuclear shape, chromosome arrangement, and local structure in specific chromosomal regions. Specifically, all chromosomes display a right-handed coiling chirality even though large differences exist in chromosome size and coiling. In each cell type, centric heterochromatic regions have a unique structure and intranuclear location. The organization of nucleolar chromatin is also tissue-specific. Prothoracic and salivary gland nuclei share many general chromosome-packing motifs, whereas hindgut and especially midgut nuclei display striking departures from these regularities. Gut chromosomes often appear to break within the centric heterochromatin. In vivo observations reveal severe deformations of midgut nuclei which may account for some of their unusual properties; they also suggest that chromosome positions within the nucleus are constrained.

Chromosome Substructure

The data in Fig. 2 suggest that the $\sim\sqrt{2}$ increase of chromosome bandwidth with each DNA doubling determined from squashes (18, 28) is an accurate reflection of the situation in vivo. This value indicates that when DNA content doubles, the new chromatids are packed laterally into chromomeres at a density similar to that of the previous polyteny level. That is, as a band grows, it probably does so not by changing modes of higher-order chromatin packing but by reiterating a basic folding regime. However, chromosome length also increases as the level of ploidy is augmented (Table III). The width and length changes would be compatible if length increases are limited to interbands (also see reference 4).

An interesting result is obtained by using the $\sqrt{2}$ value to extrapolate back to the 1C chromosome present before polytenization. If a 1.5- μm width (Fig. 2) represents a 256C DNA content, the width of the 1C fiber would be ~ 94 nm. Structures precisely in this size range (80–100 nm) have been observed in *Drosophila* and human chromosomes by electron microscopy (Belmont, A., J. W. Sedat, and D. Agard, manuscript submitted for publication). Equivalently, the maximum cross-sectional area available to a single chromatid in the average polytene band can be estimated (28). A 1.5- μm -wide band containing 256 chromatids provides a maximum cross-sectional area per chromatid of $0.0069 \mu\text{m}^2$, treating the chromosome as a cylinder. This area could accommodate a cylindrical fiber with a maximum diameter of ~ 94 nm, the same value calculated above.

These calculations raise the intriguing possibility that the banded structure of the polytene chromosome represents a direct geometric amplification of a chromomeric organization in diploid chromatin. Study of polytene band/interband regions may thus provide direct insight into diploid chromatin structure. The correspondence also suggests that the full cross section of the band is packed with chromatin rather than having a toroidal organization (36). The size and arrangement of chromatid fibers within the band must also meet these boundary constraints. For example, a 50-nm fiber (36, 45) could meet the ~ 94 -nm limit by forming a flattened higher order coil or loop in which three stretches of the fiber are laterally packed across the band. On the other hand, 200-

nm chromatid fibers (45) would be too large to pack in register laterally across a band. More complex staggered packings are imaginable but would be inconsistent with the implied correspondence between a polytene band and a chromomere in the diploid nucleus. To validate these conclusions, it will be important to verify the DNA level assignments made here.

The increment in bandwidth between the two polyteny levels in salivary glands is lower than expected (Fig. 2). This may be due to incomplete band replication, which would imply that either the chromatids in a band replicate asynchronously or only a subset of the chromatids replicate at this stage. There is evidence for lateral asynchrony in salivary gland chromosome replication (30), and total replication time increases with polyteny (43). This could be due to higher polyteny chromosomes having to compete for limiting amounts of replication factors. Alternatively, a change in the mode of packing of chromatin within the bands might occur at this level of polyteny, e.g., a tighter lateral association of folded chromatids. Several other nuclear properties change concomitantly. The fraction of nuclear volume taken up by chromosomes no longer increases as chromosomes grow. This would be consistent with a shift to a more compact packing of chromatin within the chromosome. Finally, bandwidth does not correlate with chromosome length in salivary gland nuclei as it does in the other tissues, perhaps also reflecting an adjustment of chromatid packing in bands and/or interbands. Analysis of smaller salivary gland chromosomes will be needed to determine to what extent tissue-specific factors are involved in these differences rather than the level of ploidy per se.

Chromosome Coiling and Chirality

That a predominance of right-handed coils typifies all chromosomes studied, even in midgut nuclei that retain few of the properties found in the other nuclei, indicates that this chirality is a basic property of the polytene chromosome. As such, it provides another useful boundary condition for models of polytene chromosome structure. The data in this report define the characteristics of the chirality more fully. First, it is present in short, thin chromosomes of low polyteny (as low as 256C). Second, even in gut chromosomes, which are much less coiled, the infrequent gyres are almost all right-handed. Third, the chirality appears to be retained in unpaired chromosome regions, as in salivary glands (22). Finally, chromosomes can form plectonemic coils that always twist in a left-handed direction, implying that this mode of coiling is mechanistically related to right-handed solenoidal coiling.

The tight coiling of low polyteny chromosomes as well as the reduction of coiling as prothoracic gland chromosomes grow, indicates that coiling generally decreases as polyteny increases, at least in later stages. This points to an early time in the life of the cell when coiling is maximal and suggests that as the chromosome lengthens and thickens, gyres are eliminated (also see reference 4). Coiling may be a relic of mitotic chromosome spiralization (12). However, data on the regular higher-order coils in treated mitotic and meiotic chromosomes show no preferred coiling direction (31, 37). As a chirality in coiling has implications for the mechanism of chromosome condensation, our data suggest this issue deserves reinvestigation. On the other hand, chirality may develop in the interphase nucleus. If true, right-handed coils

could result from a hierarchy of chiral molecular interactions within and between chromatids, analogous to the right-handed collagen fibril. Alternatively, they may arise from the denaturation of the right-handed DNA duplex required for its templating functions; the positive torsion on either side of the denatured zone could lead to twisting or coiling of the chromosome. Such torsion can twist one DNA duplex around another during the replication of circular DNA molecules (51).

The left-handed interwound loops described here provide some support for the idea of an interphase origin for chiral coiling. Homologues in polytene nuclei are intimately synapsed along their entire length. Because they are apparently not paired in late mitosis (9), synapsis must occur during the ensuing interphase. Pairing is complete in the interwound polytene loops; thus, to generate such loops from mitotic coils requires refolding chromosomes that have only partially decondensed yet have the two homologues at least roughly synapsed. The simplest explanation is that an intrinsic torsional strain in the chromosome leads both to solenoidal coiling and occasionally to plectonemic coiling. The relic gyres seen in early prophase and then gradually eliminated would, in this view, be the remnants not of the previous mitotic spiraling (12) but of interphase coiling. We are now attempting to reconstruct early prophase chromosomes to determine whether the predicted bias in coiling direction is present.

Chromosome Positions and the Physical Properties of Interphase Nuclei

The prothoracic gland data are consistent with our earlier suggestion that features such as chromosome domain separation, Rab1 orientation, and nearest-neighbor packing of autosome arms reflect the stable maintenance of chromosome positions since the last mitosis many days before (22). Recently, Hilliker (19) has found support for this view by inducing chromosome interchanges in the salivary gland anlage of 10–14-h embryos with gamma radiation. The resulting pattern of interchanges suggested that each chromosome arm occupies a restricted domain within the nucleus at this early stage.

The telophase condition, except for the absence of homologue synapsis, may be regarded as the starting state for every interphase nucleus. Several polytene cell types appear to retain much of this condition. What happens in gut nuclei that leads to the loss of telophaselike features and apparently even chromosome breakage (but no loss of homologue pairing)? On the basis of *in vivo* observations of midguts (Fig. 11), we suggest that these changes are traceable to the severe deformations of nuclei during peristaltic contractions.

Chromosomes may be jostled into new positions at the end of mitosis, during the transition period when the spindle is depolymerizing and the nucleus is being reestablished. The first gut contractions begin ~13–14 h into embryogenesis (15), close to the time of the last gut mitoses. This hypothesis, while plausible, raises a paradox when applied to centric heterochromatin breakage because severing chromosomes in diploid cells that must later divide will surely lead to chromosome loss. An alternative explanation is that the nucleus responds to stresses in a manner similar to certain pliant composite materials in which a three-dimensional system of high modulus fibers is embedded in a viscoelastic gel phase

(52). Nucleoplasm has gellike properties (11), and the polytene chromosome, with its many aligned chromatids, might be expected to behave as a crystalline polymer (52). As they grow, chromosomes may gradually move under the continual stresses. When the number of aligned chromatids increases, the tensile strength of the euchromatic segments will increase, but the unreplicated heterochromatin at their bases may simultaneously become susceptible to fracture under stress. This interpretation predicts that early midgut nuclei will be much more like nonstressed tissues, e.g., without chromosome intertwinings or breaks.

Chromatin Organization of Centric Heterochromatin and Nucleoli

The chromocenter is made up of two zones with distinct structural and functional properties (see reference 48). The centric heterochromatin seen in mitotic chromosomes is thought to be confined to the highly underreplicated and transcriptionally inactive α -heterochromatin in polytene cells. Within this region on the sex chromosomes is the nucleolar organizer, containing the ribosomal RNA cistrons, which are replicated to a higher level than the surrounding satellite-rich sequences. The poorly banded β -heterochromatin, interposed between the α -heterochromatin and the banded euchromatin, replicates in synchrony with euchromatin and is transcriptionally active.

The structural variation seen between chromocenters in different tissues is primarily in β -heterochromatin. Such differences were unexpected inasmuch as the banding pattern in different tissues is very similar (23, 41). Because in some tissues the chromocenter is in the nuclear interior, nuclear envelope interaction cannot be directly responsible for its heterochromatic properties. Laird (27) has proposed a model in which a nested set of stalled replication forks mark the boundary between euchromatin and unreplicated heterochromatin and between the ribosomal RNA gene cluster and the surrounding heterochromatin. Such a structure has been observed for amplified chorion genes (38). This unusual DNA organization may make the large-scale structure especially sensitive to tissue-specific differences in underlying levels of chromatin order. Nucleosome linker length varies widely between cell types, and the structure of the “30-nm fiber” can change with linker length, particularly in the crossed linker model (54). This change may translate into the tissue-specific morphology we observe. Another possibility is that centric sequences are differentially replicated in different tissues. It is known that satellite sequences in various polytene or polyploid tissues of *Drosophila* adults are replicated to different extents (48).

Position-effect variegation refers to the inactivation of a euchromatic gene that is placed next to a heterochromatic breakpoint. It appears to occur by the propagation of a heterochromatic structure into the gene (49). From the tissue-specific structure of chromocentral heterochromatin, one may predict that the ability of a heterochromatic structure to propagate into a nearby gene that is active in several tissues would differ in each. Tissue differences in position effect variegation have in fact been documented (49). Certain heterochromatin-specific nonhistone proteins may be involved in this phenomenon (25), and it will be interesting to learn whether these proteins differ in distribution or quantity between cell types.

Nucleolar DNA consists primarily of preribosomal RNA-coding sequences separated by spacer sequences (39). Conceivably, specific subsets of nucleolar sequences, e.g., the spacers, organize differently in each tissue to yield distinctive chromatin morphologies (Fig. 8). Alternatively, the differential replication of intron⁺ and intron⁻ ribosomal genes (16) may be under tissue-specific control, resulting in altered chromatin morphologies. Evidence that this occurs has been marshalled to explain the narrow range of pleiotropic effects seen with rDNA deletions (13). These ideas can be tested by in situ hybridization with the appropriate DNA probes.

In summary, we find that chromosomes and particular chromosome regions have tissue-specific organizational features. Variations between cell types include potentially functionally significant differences in chromatin structure in the nucleolus and in centric heterochromatin and differences that probably reflect a mechanically active tissue environment. A regular means of folding DNA into chromosomes may exist that leads to an apparently constant packing density within bands as nuclei grow. Size measurements also suggest an unexpected correspondence between diploid and polytene higher-order chromatin structure. A right-handed coiling chirality typifies chromosomes from all tissues. This may be relevant to the mechanism of mitotic chromosome condensation or to aspects of interphase chromosome structure and DNA topology. Many of the issues brought to the fore by these data can be further examined by a comparative three-dimensional analysis of chromosome substructure, particularly of chromocentral chromatin and band/interband regions. We are developing both high-resolution optical and electron-microscopic reconstruction techniques to allow this.

We thank Andrew Belmont, Mary Rykowski, and David Agard for comments on the manuscript, Lou Reichardt for use of the VCR, and Bruce Alberts for use of the microinjection apparatus.

This work was funded by grant GM25101 from the National Institutes of Health. Dr. Hochstrasser was supported by a National Science Foundation predoctoral fellowship.

Received for publication 24 October 1986.

References

- Aggarwal, S. K., and R. C. King. 1969. A comparative study of the ring glands from wild-type and 1(2)gl mutant *Drosophila melanogaster*. *J. Morphol.* 129:171-200.
- Ananiev, E. V., and V. E. Barsky. 1985. Elementary structures in polytene chromosomes of *Drosophila melanogaster*. *Chromosoma (Berl.)*. 93: 104-112.
- Ashburner, M., and H. D. Berendes. 1978. Puffing of polytene chromosomes. In *The Genetics and Biology of Drosophila*. Volume 2B. M. Ashburner and T. R. F. Wright, editors. Academic Press, Inc., New York. 316-395.
- Beermann, W. 1962. Riesenchromosomen. *Protoplasmatologia*. 6C:1-161.
- Braun, W. 1983. Representation of short- and long-range handedness in protein structures by signed distance maps. *J. Mol. Biol.* 163:613-621.
- Bridges, C. B. 1935. Salivary chromosome maps. *J. Hered.* 26:60-64.
- Bridges, P. N. 1942. A new map of the salivary gland 2L-chromosome of *Drosophila melanogaster*. *J. Hered.* 33:403-408.
- Burgoyne, L. A., M. A. Wagar, and M. R. Atkinson. 1971. Calcium-dependent priming of DNA synthesis in isolated rat liver nuclei. *Biochem. Biophys. Res. Commun.* 39:254-259.
- Cooper, K. W. 1948. The evidence for long-range specific attractive forces during the somatic pairing of Dipteran chromosomes. *J. Exp. Zool.* 108: 327-332.
- Cozzarelli, N. R., M. A. Krasnow, S. P. Gerrard, and J. H. White. 1984. A topological treatment of recombination and topoisomerases. *Cold Spring Harbor Symp. Quant. Biol.* 49:383-400.
- D'Angelo, E. G. 1950. Salivary gland chromosomes. *Ann. N. Y. Acad. Sci.* 50:910-919.
- Darlington, C. D. 1965. Recent Advances in Cytology. J. & A. Churchill Ltd., London.
- DeSalle, R., and A. R. Templeton. 1986. The molecular through ecological genetics of abnormal abdomen. III. Tissue-specific differential replication of ribosomal genes modulates the abnormal abdomen phenotype in *Drosophila mercatorum*. *Genetics*. 112:877-886.
- Echalier, G. and A. Ohanessian. 1970. In vitro culture of *Drosophila melanogaster* embryonic cells. *In Vitro (Rockville)*. 6:162-172.
- Ede, D. A., and S. J. Counce. 1956. A cinematographic study of the embryology of *Drosophila melanogaster*. *Wilhelm Roux' Arch. Entwicklungsmech. Org.* 148:402-415.
- Endow, S. A. 1983. Nucleolar dominance in polytene cells of *Drosophila*. *Proc. Natl. Acad. Sci. USA*. 80:4427-4431.
- Filshie, B. K., D. F. Poulson, and D. F. Waterhouse. 1971. Ultrastructure of the copper-accumulating region of the *Drosophila* larval midgut. *Tissue & Cell*. 3:77-102.
- Hartmann-Goldstein, I., and D. J. Goldstein. 1979. Effect of temperature on morphology and DNA-content of polytene chromosomes in *Drosophila*. *Chromosoma (Berl.)*. 71:333-346.
- Hilliker, A. J. 1986. Assaying chromosome arrangement in embryonic interphase nuclei of *Drosophila melanogaster* by radiation-induced interchanges. *Genet. Res.* 47:13-18.
- Hochstrasser, M. 1987. Chromosome structure in 4 wild-type polytene tissues of *Drosophila melanogaster*: the 87A and 87C heat shock loci are induced unequally in the midgut in a manner dependent on growth temperature. *Chromosoma (Berl.)*. In press.
- Hochstrasser, M., and J. W. Sedat. 1987. Three-dimensional organization of *Drosophila melanogaster* interphase nuclei. II. Chromosome spatial organization and gene expression. *J. Cell Biol.* 104:1471-1482.
- Hochstrasser, M., D. Mathog, Y. Gruenbaum, H. Saumweber, and J. W. Sedat. 1986. Spatial organization of chromosomes in the salivary gland nuclei of *Drosophila melanogaster*. *J. Cell Biol.* 102:112-123.
- Holden, J. J., and M. Ashburner. 1978. Patterns of puffing activity in the salivary gland chromosomes of *Drosophila*. IX. The salivary and prothoracic gland chromosomes of a dominant temperature sensitive lethal of *D. melanogaster*. *Chromosoma (Berl.)*. 68:205-227.
- Hsu, T. C., J. E. K. Cooper, M. L. Mace, and B. R. Brinkley. 1971. Arrangement of centromeres in mouse cells. *Chromosoma (Berl.)*. 34:73-87.
- James, T. C., and S. C. R. Elgin. 1986. Identification of a nonhistone chromosomal protein associated with heterochromatin in *Drosophila melanogaster* and its gene. *Mol. Cell. Biol.* 6:3862-3872.
- Koller, P. C. 1935. The internal mechanics of the chromosomes. IV. Pairing and coiling in salivary gland nuclei of *Drosophila*. *Proc. R. Soc. Lond. B Biol. Sci.* 118:371-396.
- Laird, C. 1973. DNA of *Drosophila* chromosomes. *Annu. Rev. Genet.* 7: 177-204.
- Laird, C. D., Ashburner, M., and Wilkinson, L. 1980. Relationship between relative dry mass and average band width in regions of polytene chromosomes of *Drosophila*. *Chromosoma (Berl.)*. 76:175-189.
- Lakhotia, S. C., and J. Jacob. 1974. EM autoradiographic studies of polytene nuclei of *Drosophila melanogaster*. *Exp. Cell Res.* 86:253-263.
- Lakhotia, S. C., and P. Sinha. 1983. Replication in *Drosophila* chromosomes. X. Two kinds of active replicons in salivary gland polytene nuclei and their relation to chromosomal replication patterns. *Chromosoma (Berl.)*. 88:265-276.
- Manton, I., and J. Smiles. 1943. Observations on the spiral structure of somatic chromosomes in *Osmunda* with the aid of ultraviolet light. *Ann. Bot. (Lond.)*. 7:195-212.
- Mathog, D. 1985. Light microscope based analysis of three-dimensional structure: applications to the study of *Drosophila* salivary gland nuclei. II. Algorithms for model analysis. *J. Microsc. (Oxf.)*. 137:254-275.
- Mathog, D., M. Hochstrasser, and J. W. Sedat. 1985. Light microscope based analysis of three-dimensional structure: applications to the study of *Drosophila* salivary gland nuclei. I. Data collection and analysis. *J. Microsc. (Oxf.)*. 137:241-253.
- Mathog, D., M. Hochstrasser, Y. Gruenbaum, H. Saumweber, and J. Sedat. 1984. Characteristic folding pattern of the polytene chromosomes in *Drosophila* salivary gland nuclei. *Nature (Lond.)*. 308:414-421.
- Moens, P. B., and K. Church. (1977). Centromere sizes, positions, and movements in the interphase nucleus. *Chromosoma (Berl.)*. 61:41-48.
- Mortin, L. I., and J. W. Sedat. 1982. Structure of *Drosophila* polytene chromosomes: evidence for a toroidal organization of the bands. *J. Cell Sci.* 57:73-113.
- Ohnuki, Y. 1968. Structure of chromosomes. I. Morphological studies of the spiral structure of human somatic chromosomes. *Chromosoma (Berl.)*. 25:402-428.
- Osheim, Y. N., and O. L. Miller, Jr. 1983. Novel amplification and transcriptional activity of chorion genes in *Drosophila melanogaster* follicle cells. *Cell*. 33:543-553.
- Pardue, M. L., S. A. Gerbi, R. A. Eckhardt, and J. G. Gall. 1970. Cytological localization of DNA complementary to ribosomal RNA in polytene chromosomes of Diptera. *Chromosoma (Berl.)*. 29:268-290.
- Poulson, D. F., and D. F. Waterhouse. 1960. Experimental studies on pole cells and midgut differentiation in Diptera. *Aust. J. Biol. Sci.* 13:541-

41. Richards, G. 1980. The polytene chromosomes in the fat body nuclei of *Drosophila melanogaster*. *Chromosoma (Berl.)*. 79:241-250.
42. Robertson, C. W. 1936. The metamorphosis of *Drosophila melanogaster*, including an accurately timed account of the principal morphological changes. *J. Morphol.* 59:351-399.
43. Rudkin, G. T. 1972. Replication in polytene chromosomes. In *Developmental Studies on Giant Chromosomes. Results and Problems in Cell Differentiation*. W. Beerman, editor. Springer-Verlag, Berlin. 59-85.
44. Sachs, L. 1983. *Applied Statistics*. Springer-Verlag, New York.
45. Sedat, J. W., and L. Manuelidis. 1978. A direct approach to the structure of eukaryotic chromosomes. *Cold Spring Harbor Symp. Quant. Biol.* 42: 331-350.
46. Semionov, E. P., and N. Kh. Kirov. 1986. Increased number of nucleoli in the salivary gland cells of *Drosophila melanogaster* under conditions of rDNA dose compensation. *Chromosoma (Berl.)*. 93:477-482.
47. Sonnenblick, B. P. 1950. The early embryology of *Drosophila melanogaster*. In *Biology of Drosophila*. M. Demerec, editor. J. Wiley & Sons, New York. 62-167.
48. Spear, B. B. 1977. Differential replication of DNA sequences in *Drosophila* chromosomes. *Am. Zool.* 17:695-706.
49. Spofford, J. B. 1976. Position effect variegation in *Drosophila*. In *The Genetics and Biology of Drosophila*. Volume 1C. M. Ashburner and E. Novitski, editors. Academic Press, Inc., New York. 955-1018.
50. Strasburger, M. 1932. Bau, Funktion und Variabilität des Darmtractus von *Drosophila melanogaster* Meigen. *Z. Wiss. Zool.* 140:539-649.
51. Sundin, O., and A. Varshavsky. 1981. Arrest of segregation leads to accumulation of highly intertwined catenated dimers: dissection of the final stages of SV40 DNA replication. *Cell*. 25:659-669.
52. Wainwright, S. A., W. D. Biggs, J. D. Currey, and J. M. Gosline. 1982. *Mechanical Design in Organisms*. John Wiley & Sons, New York.
53. Welch, R. M. 1957. A developmental analysis of the lethal mutant 1(2)gl of *Drosophila melanogaster* based on cytophotometric determination of nuclear desoxyribonucleic acid (DNA) content. *Genetics*. 42:544-559.
54. Williams, S. P., B. D. Athey, L. J. Muglia, R. S. Schappe, A. H. Gough, and J. P. Langmore. 1986. Chromatin fibers are left-handed double helices with diameter and mass per unit length that depend on linker length. *Biophys. J.* 49:233-248.
55. Zelechowska, M. G., and E. F. Potworoski. 1985. Improved adhesion of ultrathin sections to filmless grids. *J. Electron Microsc. Tech.* 2:389-390.
56. Zhimulev, I. F., V. F. Semeshin, V. A. Kulchicov, and E. S. Belyaeva. 1982. Intercalary heterochromatin in *Drosophila*. I. Localization and general characteristics. *Chromosoma (Berl.)*. 87:197-228.